Journal of Power Sources 239 (2013) 244–252

Contents lists available at SciVerse ScienceDirect

Journal of Power Sources

journal homepage: www.elsevier.com/locate/jpowsour

Evaluation of properties and performance of nanoscopic materials in vanadium diboride/air batteries

Christopher Rhodes [a,*], Jessica Stuart [b], Ruben Lopez [a], Xuguang Li [a], Mahesh Waje [a], Matthew Mullings [a], Jason Lau [b], Stuart Licht [b,**]

[a] Lynntech, 2501 Earl Rudder Fwy S, College Station, TX 77845, USA
[b] Department of Chemistry, The George Washington University, 2121 Eye Street NW, Washington, DC 20052, USA

HIGHLIGHTS

- VB_2/air batteries containing nanoscopic VB_2 anodes have significantly higher voltages and capacities than cells containing macroscopic VB_2 anodes.
- The nanoscale thickness of the zirconia layer on the VB_2 nanomaterial may facilitate rapid discharge through the coating.
- The higher performance of the VB_2 nanoscopic material may result from the combination of the nanomaterial's higher surface area and higher electronic conductivity.
- Electrochemical impedance analysis showed that charge transfer resistance increases from charge to discharge for cells containing both macroscopic and nanoscopic VB_2.

ARTICLE INFO

Article history:
Received 22 October 2012
Received in revised form
13 March 2013
Accepted 15 March 2013
Available online 28 March 2013

Keywords:
Vanadium diboride/air batteries
Nanomaterials
Electrochemical properties
High energy density power sources

ABSTRACT

The unique eleven electron per molecule electrochemical oxidation of vanadium diboride (VB_2) combined with an air cathode provides VB_2/air batteries that have extremely high theoretical energy densities. Testing of VB_2/air cells at various discharge times showed that VB_2/air batteries containing nanoscopic VB_2 anodes provide higher capacities and voltages than cells containing macroscopic VB_2 anodes. The structure and properties of nanoscopic VB_2 were compared with those of macroscopic VB_2 to provide further insight into the enhanced electrochemical performance of the nanomaterial. From nitrogen physisorption and electrical conductivity measurements, we determined that the higher performance of the nanoscopic VB_2 material compared with the macroscopic VB_2 material may result from the combination of the nanomaterial's higher surface area and higher electronic conductivity. The thickness of the zirconia layer applied to prevent corrosion in alkaline electrolyte was shown by transmission electron microscopy and energy dispersive X-ray spectroscopy to be ca. 3–40 nm which may allow rapid discharge through the coating. Electrochemical impedance spectroscopy results showed that for cells containing both the macroscopic and the nanoscopic materials the resistance associated with charge transfer increases during the discharge process. The results provide a basis for further development of high energy and power density VB_2/air batteries.

1. Introduction

For over a century, metallic zinc has been predominantly used as an anode material in almost all aqueous primary systems due to zinc metal's high two-electron oxidation capacity. The zinc–carbon battery, known as the Leclanché cell, was first introduced in the 19th century, as a low-cost solution for early energy storage needs. The zinc cell, which produced approximately 65 Wh kg^{-1}, was ideal only for low rate discharges. Precipitation of side reaction products creates an increase in cell resistance and contributes to cell leakage, resulting in instability [1,2]. Until the development of the zinc/alkaline/manganese dioxide battery and the zinc/air cell, there was little improvement in primary batteries. The alkaline Zn/MnO_2 cell has since dominated primary electrochemical storage, offering 145 Wh kg^{-1}. Although more expensive than the zinc–carbon battery, the alkaline cell improved performance by increasing energy densities and power capabilities. The zinc/air battery, similar to a fuel cell, offered further improvements exhibiting the highest

* Corresponding author. Tel.: +1 979 764 2313; fax: +1 979 764 2343.
** Corresponding author. Tel.: +1 703 726 8225; fax: +1 202 994 5873.
E-mail addresses: christopher.rhodes@lynntech.com, cprhodes@suddenlink.net (C. Rhodes), slicht@gwu.edu (S. Licht).

0378-7753/$ – see front matter © 2013 Elsevier B.V. All rights reserved.
http://dx.doi.org/10.1016/j.jpowsour.2013.03.071

energy density of many primary systems. The zinc/air cell is limited in power output by the air cathode. For a wide range of electronic devices, it would be useful to achieve even higher energy densities than that of the zinc/air battery [3]. Most metal/air batteries to date, including the zinc/air cell, have been unsuccessful in reaching the high energy densities possible by multi-electron oxidations, due to material passivation or chemical instabilities [4].

To provide high energy density cells, in recent years there has been an immense effort to successfully develop a high capacity anode through multi-electron charge storage processes [5]. Vanadium diboride (VB_2) undergoes an extraordinary multiple electron oxidation process, which to its completion involves an 11 electron per molecule oxidation, including oxidation of the tetravalent transition metal ion, V($+4 \rightarrow +5$), and each of the two boron's $2 \times B(-2 \rightarrow +3)$ [6]. VB_2 has an intrinsic gravimetric capacity of 4060 Ah kg^{-1} which is five-fold higher than that of the Zn anode electrode (820 Ah kg^{-1}). The intrinsic volumetric anodic capacity of the VB_2 anode (20.7 kAh L^{-1}) is ten-fold higher than that of the lithium anode (2.06 kAh L^{-1}).

The VB_2 anode can be coupled with available air to provide extremely high energy density VB_2/air batteries [6]. The anode half cell, cathode half cell, and full cell reactions based on generalized discharge products [7] are as follows:

$$\text{Anode: } VB_2 + 11OH^- \rightarrow 1/2V_2O_5 + B_2O_3 + 11/2H_2O + 11e^- \quad (1)$$

$$\text{Cathode: } O_2 + 2H_2O + 4e^- \rightarrow 4OH^- \quad (2)$$

$$\text{Cell: } 2VB_2 + 11/2O_2 \rightarrow 2B_2O_3 + V_2O_5 \quad E_{cell} = 1.55\ V \quad (3)$$

The VB_2/air battery has a theoretical discharge potential of 1.55 V, as calculated from the thermodynamic free energy of the cell reactants and products [7]. The VB_2/air cell's intrinsic volumetric energy density of 32 kWh L^{-1} is substantially greater than that of gasoline (<10 kWh L^{-1}) [6,8]. VB_2/air batteries have an intrinsic specific energy of 5300 kWh kg^{-1}, which is four times higher than the theoretical specific energy of zinc/air batteries (1353 kWh kg^{-1}).

The VB_2/air couple uses an alkaline electrolyte of KOH/NaOH, and oxygen from the air reacts at the cathode similar to that of the zinc/air cell [1]. While concentrated aqueous hydroxide electrolytes ranging from 8 M to saturated in NaOH or KOH yield a similar electrochemical discharge in the VB_2/air cell, we have recently observed that a mixture of NaOH and KOH yields marginally improved high rate performance [7] compared to the earlier pure NaOH electrolyte [6,8] and have continued with this mixed electrolyte in this study. The VB_2/air cell shows an experimental open circuit potential of ~1.3 V, and under load, the cell can release its capacity over a flat, remarkably singular discharge potential plateau. Previous work by Licht et al. has shown that although VB_2 is susceptible to corrosion in alkali media, a zirconia overlayer on VB_2 prevents this corrosion [6]. Prior work demonstrated that thin zirconia coatings on macroscopic alkaline battery materials do not impede charge transfer at rates tested, but provide significant stability benefits [6,9–11]. Therefore, coating the anode material with a zirconia layer has been developed as a strategy to stabilize VB_2 against corrosion in the alkaline electrolyte.

Recently, Licht et al. have developed nanoscopic VB_2 materials prepared using mechanochemical processes and showed that at slow discharge times of between eight and ten hours cells containing nanoscopic VB_2 exhibited higher voltages and discharge capacities compared with cells containing macroscopic VB_2 [7]. Operating at slow discharge times is useful for many applications such as portable electronics and hearing aids. However, for many applications operating at rapid discharge times is needed for full discharge, partial discharge or high power pulses. Achieving cells that provide high performance at high discharge rates requires material properties and an electrode structure designed for high power operation.

Preliminary results from previous works established by Licht et al. suggest that zirconia-coated nanoscopic VB_2 will outperform the uncoated and macroscopic materials [5–7]. Based on the improved performance of the nanoscopic VB_2 at slow discharge times we postulated that at high discharge rates nanoscopic VB_2 would provide improved performance compared with macroscopic VB_2.

In this study, we explored the properties and performance of nanoscopic VB_2 materials and compared the results obtained with macroscopic VB_2 materials. Electrochemical testing was performed to determine the performance of nanoscopic VB_2 at rapid discharge times. Material properties were investigated using microscopy, electrical measurements, nitrogen physisorption, and electrochemical impedance spectroscopy to determine the reason for the improved performance of cells containing the nanomaterials. The specific material properties of the nanoscopic VB_2 have not been previously studied, and a greater understanding of the VB_2/air system provides the ability to further improve the performance of this interesting multi-electron charge storage material [6].

2. Experimental

2.1. Vanadium diboride synthesis

Nanoscopic VB_2 was synthesized mechanochemically using vanadium powder (Alfa Aesar) and boron powder (Alfa Aesar) based on results previously published by Licht et al. [7]. In a controlled argon atmosphere glovebox system (Vacuum Atmospheres, Nexus-II), 0.500 g of vanadium and 0.212 g of boron power were measured and transferred into a tungsten carbide milling chamber along with ten tungsten carbide balls, ten millimeters in diameter. The milling vessel was sealed, removed from the glovebox, and placed into a Retsch PM 100 planetary ball mill set to 600 rpm and allowed to run for four hours. After the vanadium diboride cooled to room temperature, the material was then collected in the glovebox into a round bottom flask, and the mass was measured. A zirconium oxide layer was formed by adding 3.5% by weight (or as noted in the text) zirconium chloride (Acros Organics), following the procedure outlined by Licht et al. with the exception of adding ten milliliters diethyl ether to the round bottom flask; the 3.5 wt% $ZrCl_4$ addition forms a 1.9 wt% ZrO_2 overlayer [9]. After one hour of mixing on a stir plate, the ether was evaporated using a rotary evaporator and collected. For comparison, macroscopic VB_2 was obtained from American Elements and was coated in a similar manner as described above.

2.2. Electrochemical testing

Panasonic 675 Zinc/Air batteries (Panasonic Corporation, Japan) were used for cell fabrication. The Zn anode of the Panasonic cells was removed by opening the existing cell and removing the anode active material. The separator and cathode were used as received for the VB_2/air battery as further described in Supplemental data. The VB_2 anode was fabricated by mixing 30 wt% carbon black (Timcal Super-C65) with 70 wt% VB_2 (as synthesized coated nanoscopic material or macroscopic material) and spread on the cap with isopropyl alcohol. The electrode area was approximately 0.57 cm^2. For all cells, the mass loading was 1.2 ± 0.1 mg, with the exception of the nanoscopic cells discharged at 3000 Ω, which had an average mass loading of 0.8 mg. The electrolyte, 27 μL of a mixture of 4 M KOH and 4 M NaOH, was applied to the separator. Excess electrolyte was removed using a cotton swab prior to closing each cell. The cell was then closed with the cap in reverse so that

the anodic material was in contact with the electrolyte. Once the fabrication process had been completed, cells were placed on a holder and discharged at constant loads of 3000 Ω, 1000 Ω, 600 Ω, and 200 Ω using an Arbin Instruments battery tester controlled by MITS Pro software. The discharge of each cell contained an initial rest step of 10 min during which the cells were allowed to equilibrate. At the end of the equilibration step, the open circuit potential was recorded. The equilibrated cells were then discharged under a constant load. Coulombic efficiency was calculated as the percentage of the measured capacity compared to the theoretical anode eleven electron discharge capacity of 4060 Ah kg^{-1}.

The average theoretical cell capacity was 4.5 mAh based on the measured amount of VB_2 and the theoretical specific capacity of VB_2. The average experimentally determined capacity was 2.5 mAh using the mass of VB_2 and the measured capacities. VB_2/air cells with theoretical capacities of between 5 mAh and 50 mAh have been previously reported by the authors [6–8]. The lower end of these capacities was selected for initial testing of the rate capabilities to allow measurement of the properties of VB_2 within relatively thin electrode films ($\sim$26 μm-thick). The information obtained provides a basis for designing thicker electrodes which could be used for cells with practical capacities required for various devices.

2.3. Microscopy and energy dispersive X-ray analysis

Transmission electron microscopic (TEM) measurements were performed using a FEI Tecnai G2 F20 transmission electron microscope, equipped with Schottky-type field emission gun, X-twin objective lenses, an energy dispersive X-ray spectrometer (EDS), and a scanning TEM (STEM) unit with high-angle annular dark-field (HAADF) detector operating at 200 kV. Samples were prepared by sonication of the VB_2 material in ethanol for 10 min and dropwise addition of the sample onto a carbon-coated 400 mesh Cu grid followed by solvent evaporation in air.

2.4. Electrical conductivity measurements

A two-electrode powder conductivity measurement apparatus, fabricated as per the design developed by Holmberg and Yan [12], was used for the measurement of the electrical conductivity of the VB_2 materials. Powder samples were loaded in small cylinders (φ = 0.159 cm) which were contacted by two electrodes (gold-plated stainless steel rods) on either side. The powders were loaded and measurements were taken in an inert atmosphere glovebox in order to eliminate potential effects of atmospheric exposure. The powder was compressed to a torque of 2.26 N-m by tightening the fixture screws, corresponding to a pressure of 189–283 MPa on the powder samples. The length of sample within the cylinders was between 0.4 and 0.6 cm. The resistance of the powder sample was then measured with an Agilent milliohmmeter 4338B (1 kHz). Data was also obtained using potentiostatic two electrode electrochemical impedance spectroscopy measurements (Princeton Applied Research, VersaStat) to validate the results obtained using the milliohmmeter. As a reference, the conductivity of Vulcan XC-72 carbon was obtained and compared to reported values. The electrical conductivity, σ, expressed in the unit S cm^{-1} was obtained from the experimentally determined resistance, the area, and the measured length using the equation:

$$\sigma = \frac{l}{RA} \tag{4}$$

where l is the compressed length of the sample in cm, R is the measured resistance in Ω, and A is the cross-sectional area of the electrodes.

2.5. Nitrogen physisorption measurements

Nitrogen physisorption measurements were obtained using a Micromeritics Tristar 3000 surface area porosity analyzer. Samples were prepared and loaded within an inert atmosphere glovebox. Initial weights were taken of sample material before degassing for cross-reference. Samples were degassed at two stages. The samples were taken from ambient temperature to 30 °C using a 10 °C min^{-1} ramp rate and held at 30 °C for 10 min. The second stage involved heating at 10 °C min^{-1} to either 50 °C or 100 °C followed by hold a temperature of either 50 °C or 100 °C for 4 h. Samples were then reweighed, recorded and analyzed.

2.6. Electrochemical impedance spectroscopy (EIS)

Two-point probe electrochemical impedance spectroscopy (EIS) measurements were obtained for the VB_2/air cells using a Princeton Applied Research (PAR) VersaStat MC potentiostat operated with VersaStudio software. An applied root mean square amplitude of 50 mV was used over the frequency range of 1.0 MHz–0.1 Hz, and data was taken at open circuit potential in either the charged or discharged state. The experimental impedance data was fit using ZSimpWin software (version 3.21, Princeton Applied Research) with an equivalent circuit described in the text.

3. Results and discussion

3.1. Electrochemical analysis

Electrochemical testing was performed to determine the performance of VB_2/air cells containing either 1.9 wt% ZrO_2-coated macro-VB_2 or 1.9 wt% ZrO_2-coated nano-VB_2 material at different discharge times ranging from 13 h (3000 Ω) to less than 1 h (200 Ω). Data obtained for relatively slow discharge times of 8–13 h (3000 Ω) and 4 h (1000 Ω) are shown in Fig. 1. The results obtained for multiple cells provide evidence for reproducibility of the cell performance. Relatively small differences in the voltages and capacities observed for repeated cells may result from small mass differences, as well as from using cell configuration that did not result in uniform pressure applied to each cell.

From the data presented in Fig. 1, it is evident that at relatively low discharge times of between 4 and 13 h the nanoscopic VB_2 anode cells show significantly higher discharge voltages and greater discharge capacities compared with the macroscopic VB_2 anode cells. A relatively flat, discharge voltage is also evident during the discharge at low rates (specifically at 3000 Ω), occurring without voltage steps to a columbic efficiency of over 70%. This is indicative of a nearly complete oxidative charge transfer of the full VB_2 capacity of eleven electrons.

Shown in Fig. 2 are the discharge curves obtained for faster discharge times of 2 h (600 Ω) to less than 1 h (200 Ω). As evidenced by the data in Fig. 2, at higher discharge rates, the nanoscopic material also exhibits significantly higher voltages compared to the macroscopic material, similar to the results obtained at lower discharge rates. Interestingly, although the voltages are significantly higher, the capacities of the nanoscopic and macroscopic VB_2 are similar at higher discharge times. In addition, as expected the capacities for the cells at higher rates (Fig. 2) were lower than those at lower rates (Fig. 1). A number of factors including surface area and the coating may affect the reaction and influence the high rate capacities, as discussed further below.

The discharge times, voltages, specific capacities, and specific energies for the macroscopic and nanoscopic VB_2 materials at different loads are compared in Table 1. The data shows the significantly higher voltages and specific energies (anode mass

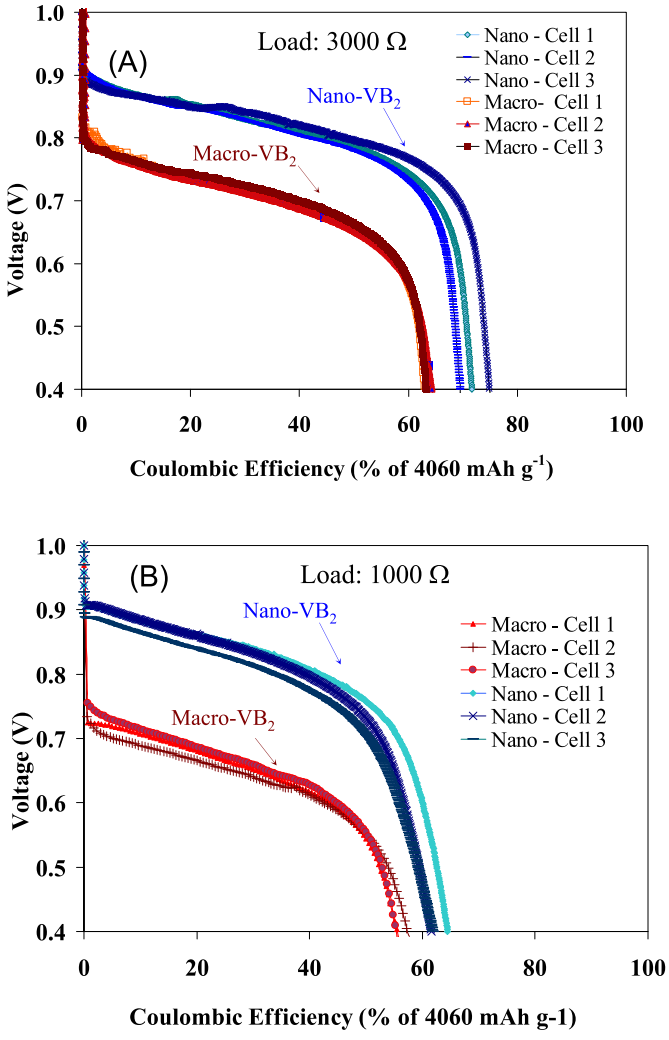

Fig. 1. Comparison of macroscopic vs. nanoscopic 1.9% ZrO_2-coated VB_2 anodes. (A) Discharge profile comparison of nanoscopic to macroscopic VB_2 for VB_2/air cells with a capacity of 5 mAh at a constant load of 3000 Ω. (B) Discharge profile comparison of nanoscopic to macroscopic VB_2 for VB_2/air cells with a capacity of 5 mAh at a constant load of 1000 Ω.

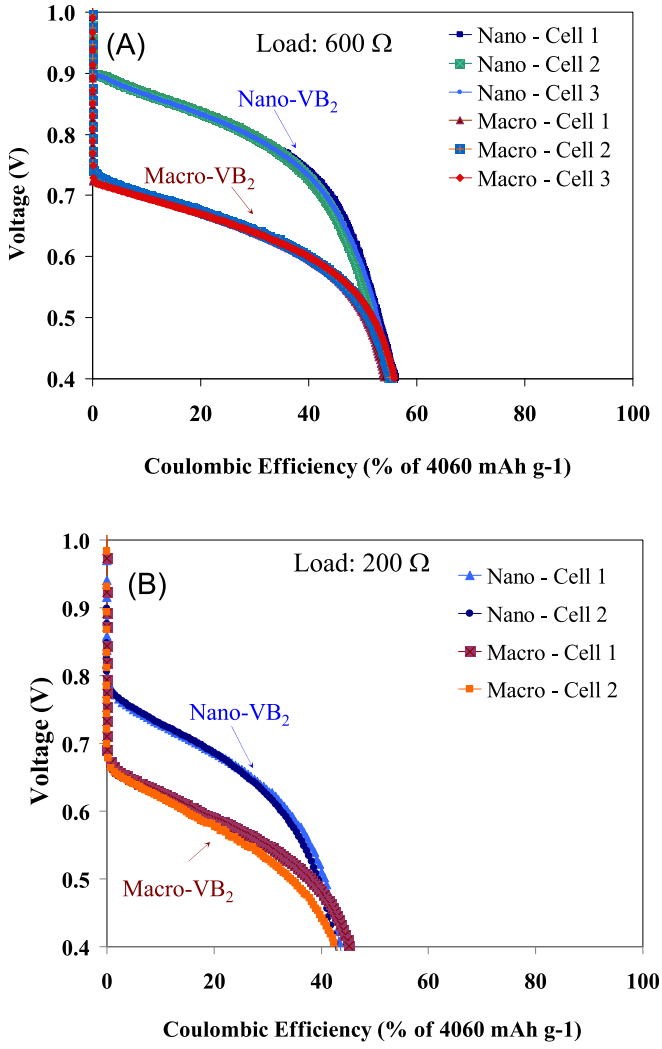

Fig. 2. Comparison of macroscopic vs. nanoscopic 1.9% ZrO_2-coated VB_2 anodes. (A) Discharge profile comparison of nanoscopic to macroscopic VB_2 for VB_2/air cells with a capacity of 5 mAh at a constant load of 600 Ω. (B) Discharge profile comparison of nanoscopic to macroscopic VB_2 for VB_2/air cells with a capacity of 5 mAh at a constant load of 200 Ω.

only) of the nanoscopic compared with the macroscopic material. The comparison of the ratios of the specific energies of the macro-VB_2 and nano-VB_2 shows that at lower discharge rates, the nano-VB_2 exhibits a higher degree of improvement in specific energy compared with the ratio observed at higher rates.

3.2. Microscopy analysis

A coating that protects the VB_2 is critical to maintaining the structure and chemical integrity of the anode material within the highly alkaline environment. The uncoated VB_2 is unstable in the alkaline environment and corrosion results in evolved hydrogen from the decomposition reaction and loss of the electrochemical capacity [6]. Zirconia is highly stable in aqueous alkaline media and maintains effective charge transfer during boride anodic discharge, preventing vanadium boride decomposition. Previous work demonstrated that for uncoated macroscopic material VB_2, stored at 45 °C for one week in contact with the electrolyte, and then discharged at room temperature loses 10% of its charge capacity, however with a 1% zirconia coating retains 100% of that capacity [6].

The morphology and thickness of the coating play an important role in the stability and electrochemical performance of the VB_2 anode and may influence performance at high discharge rates. Since the nature of the coating on the VB_2 had not been previously characterized, analysis was performed to determine the thickness and morphology of the zirconia coating on the nano-VB_2 material. For the base VB_2 material, previous work established that the uncoated nanoscopic material prepared using the mechanochemical process (high energy ball milling) results in a distribution of submicron particles in the 100–400 nm range with agglomerates of larger particles also evident [7].

To characterize the zirconia coating on the base nano-VB_2 material, transmission electron microscopic (TEM) measurements and energy dispersive X-ray spectra (EDS) were obtained. Based on the limitations of the instrument to obtain high quality images on micron-scale particles, TEM images were obtained only for the nanoscopic-coated VB_2 rather than the macroscopic-coated VB_2 since the later is composed of large micron-scale particles.

A representative TEM image of the nanoscopic VB_2 coated with 1.9 wt% ZrO_2 layer is shown in Fig. 3A. The VB_2 base material can be clearly observed in the darker region with the ZrO_2 coating layer in

Table 1
Comparison of the electrochemical performance of zirconia-coated macroscopic VB_2 and zirconia-coated nanoscopic VB_2 at various loads from 3000 Ω to 200 Ω. Values were obtained from averages of multiple cells. The specific capacity utilized the mass of the active VB_2, and the specific energy included the experimental cell voltage and the mass of the anode material only.

Load (Ω)	Material	Discharge time (h)	Voltage (V)	Specific capacity (mAh g^{-1})	% of theoretical capacity (4060 mAh g^{-1})	Specific energy (Wh kg^{-1}) (anode material)	Ratio of specific energy (nanoscopic/macroscopic)
3000	Macroscopic VB_2	13.67	0.68	2600	63	1800	1.3
	Nanoscopic VB_2	8.49	0.79	2700	72	2300	
1000	Macroscopic VB_2	3.57	0.64	2300	56	1400	1.4
	Nanoscopic VB_2	4.32	0.73	2500	63	1900	
600	Macroscopic VB_2	2.09	0.64	2200	55	1300	1.2
	Nanoscopic VB_2	2.39	0.75	2300	56	1600	
200	Macroscopic VB_2	0.71	0.60	1600	40	690	1.1
	Nanoscopic VB_2	0.61	0.66	1600	40	730	

the lighter region. The primary VB_2 particle size is in the 10–100 nm range. The thickness of the zirconia coating layer varies from ca. 3 to 40 nm. The representative EDS spectrum of nanoscopic VB_2 particles with ZrO_2 coating layer is shown in Fig. 3B. The presence of V and Zr was determined by EDS analysis of the area shown within the inset TEM image of Fig. 3B. The EDS data supports that the coating layer contains Zr.

Fig. 4A shows the representative TEM image of nanoscopic VB_2 coated with a thicker ZrO_2 layer (10 wt% $ZrCl_4$). For this sample, a higher amount of $ZrCl_4$ precursor was used to obtain a higher degree of coating. For the sample imaged, the primary VB_2 particle size is slightly larger, and the VB_2 base material and the ZrO_2 coating layer are not as distinguishable as the 3.5 wt% $ZrCl_4$ sample. The EDS spectrum of nanoscopic VB_2 particles with ZrO_2 coating layer (10 wt% $ZrCl_4$) is shown in Fig. 4B. The presence of V and Zr was determined by means of EDS. However, for this region probed the Zr content was lower since the image may have probed a significant portion of the base VB_2 in addition to the coating. As evident in Figs. 3 and 4, the zirconia coating appears to coat the entire VB_2 particles, and the coating thickness varies over the material. Interestingly, the coating is not just for discrete particles, but also results in a coating over aggregates.

3.3. Nitrogen physisorption analysis

Nitrogen physisorption measurements were obtained to determine the effect of the zirconia coating on the surface area, pore volume, and the pore size and compare the macroscopic and nanoscopic VB_2 materials. The results presented in Table 2 show that the coating affected the surface area of both the macroscopic and nanoscopic materials. For both materials, the application of the zirconia coating lowered the Brunauer, Emmett and Teller (BET) surface area compared to the uncoated materials. The results also show that the uncoated nanoscopic material prepared using high energy ball milling has a significantly larger surface area (2.84 $m^2\ g^{-1}$) compared to that of the uncoated macroscopic material (0.089 $m^2\ g^{-1}$). Similarly, the surface area of the coated nanoscopic material (0.854 $m^2\ g^{-1}$) was approximately two orders of magnitude higher compared with the surface area of the macroscopic material (0.0089 $m^2\ g^{-1}$). The data also shows that the application of the zirconia coating does reduce the surface area, as expected. For the macroscopic material, the coating decreases the surface area by an order of magnitude, while for the nanoscopic material the coating decreases the surface area by a factor of about three. For the nanomaterial, further analysis was performed to determine the effect of the coating on cumulative pore volume and pore width. Both the cumulative pore volume and average pore width decrease upon application of the coating to the base nano-VB_2. It may be significant that the cumulative surface area and cumulative pore volume between 1.7 nm and 300 nm are relatively small for the coated nano-VB_2 as well as for the macro-VB_2. Within the cumulative pore volume measurement, both mesopores (>2–50 nm) and the lower end of macropores (50 nm–500 μm) are included. In particular, high degrees of mesoporosity contribute to electrolyte access at electrochemically accessible timescales [13]. The small cumulative pore volume within the meso- and macropores may limit rapid discharge performance based on restricting electrolyte access, although the degree to which electrolyte access to the surface may be affected is not clear from present analysis. The accessibility of the underlying VB_2 to the electrolyte will also depend on the permeability of the zirconia coating to the ions within the electrolyte [14].

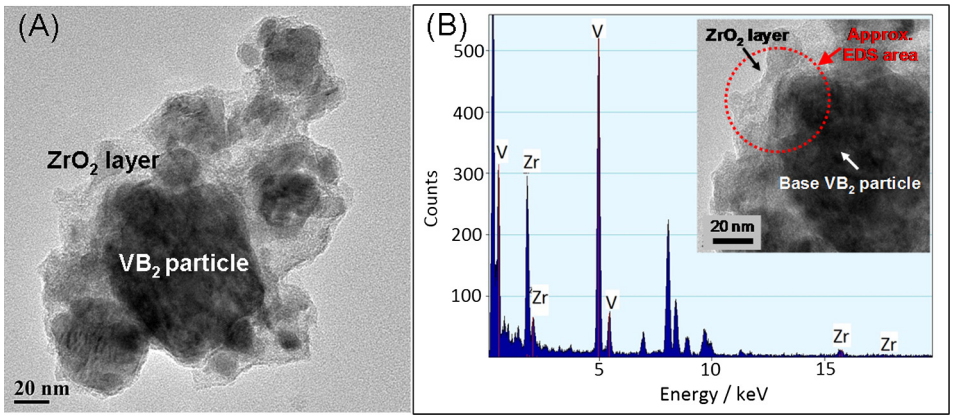

Fig. 3. (A) High resolution TEM and (B) EDS of the LT nanoscopic VB_2 particles with ZrO_2 coating layer. The inset of (B) shows the approximate EDS area which is an enlarged part of (A).

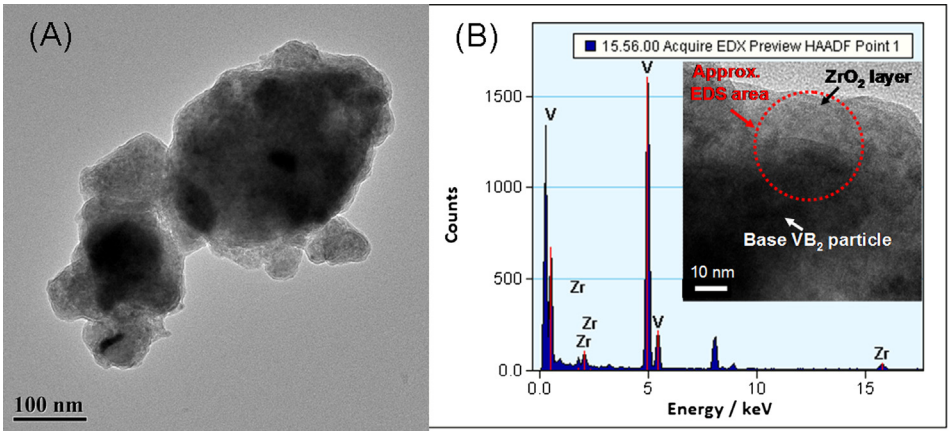

Fig. 4. (A) High resolution TEM and (B) EDS of the nanoscopic VB_2 particles with ZrO_2 coating layer. The inset of (B) shows the approximate EDS area which is an enlarged part of (A).

3.4. Electrical conductivity

Electrical conductivity measurements were obtained to determine the properties of the materials, the effect of the coating, and provide further insight into the differences between the performance of the macro-VB_2 and nano-VB_2. The electrical conductivity of the macroscopic coated, nanoscopic coated, and uncoated VB_2 materials is presented in Table 3. For comparison, the conductivities of the starting materials, elemental boron and vanadium powders, were also obtained. For the VB_2 precursors, elemental vanadium powder is highly conductive in contrast to the elemental boron powder. The coated materials show lower electrical conductivities compared with the base materials, which is expected based on the application of an electronically insulating ZrO_2 material. The results also show that the nanoscopic material has a significantly higher electronic conductivity compared to the macroscopic material, both for the uncoated and coated material, presumably related to the improved conductive matrix due to the tighter packing and larger number of interparticle contacts assessable to smaller particles. Interestingly, X-ray diffraction shows that the nanomaterial is not as highly crystalline as the macroscopic material [7]. To our knowledge, the electrical conductivity of nanoscopic VB_2 has not been previously reported. The VB_2 electrical conductivities (67–230 S cm^{-1}) are higher than the electrical conductivity of carbons typically used for electrochemical cells (ca. 0.3–2.0 S cm^{-1}) [15,16]. The higher electrical conductivity of the nano-VB_2 compared with the macro-VB_2 likely contributes to the higher voltage (i.e. lower resistance) observed within the electrochemical testing.

Table 2
Nitrogen physisorption measurements of macroscopic uncoated VB_2, macroscopic-coated VB_2, nanoscopic uncoated VB_2 and nanoscopic-coated VB_2.

Category	Parameter	Macroscopic		Nanoscopic	
		Uncoated	Coated	Uncoated	Coated
Surface area	BET surface area (m^2 g^{-1})	0.089	0.0089	2.84	0.854
	t-plot micropore area (m^2 g^{-1})	0.828	0.469	0.870	0.123
	Cumulative surface area (m^2 g^{-1}) [a]	N/A	N/A	2.57	0.251
Pore volume	Cumulative pore volume (cm^3 g^{-1}) [b]	N/A	N/A	4.29×10^{-3}	4.62×10^{-4}
Pore size	Average pore width (nm) [c]	N/A	N/A	1.8	1.1

[a] Barrett, Joyner and Halenda (BJH) adsorption; pores between 1.7 nm and 300 nm diameter.
[b] BJH adsorption; between 1.7 nm and 300 nm diameter.
[c] Adsorption (4V/A by Brunauer, Emmett and Teller (BET)).

3.5. Electrochemical impedance analysis

Electrochemical impedance spectroscopy was performed of the VB_2/air cells to allow comparison of the cell impedance in the charged state and after discharge and permit comparison of the macroscopic and nanoscopic VB_2. Shown in Fig. 5 is the complex (Nyquist) impedance plot of a representative charged VB_2/air cell containing nanoscopic VB_2 material. The complex impedance plot shows three regions of interest: (i) the high frequency x-axis intercept (Fig. 5B), (ii) the high frequency semicircle (Fig. 5B), and (iii) the low frequency region (Fig. 5A).

Based on the observed features, the equivalent circuit shown in Fig. 6 was used for fitting the experimental electrochemical impedance data. Similar equivalent circuits have been used to describe the impedance response of Zn/air batteries and related systems [17–19]. Within this equivalent circuit, R_s describes the series resistance, which includes contact resistances and the bulk electrolyte resistance. The dominant contribution to R_s is the electrolyte resistance, and the value for R_s can be determined from the point of intersection of the high frequency semicircle and the x-axis.

The mid-frequency semicircle (Fig. 5B) can be described by a resistor (R_1) in parallel with a constant phase element (Q_1). The resistance R_1 is attributed to the charge transfer resistance [20]. In this case, R_1 includes the resistances associated with ion transport through the coating and VB_2. The capacitive element indicates charge polarization coupled with the charge transfer process and has been attributed to a double layer capacitance [20]. A constant phase element was used rather than a single capacitor to account for the distribution of capacitances, which may result from the distribution of particle sizes. This combination of a resistor and capacitor in parallel is characteristic of a kinetically controlled reaction [21]. There may be multiple parallel R–C elements associated with the various elements of the charge transport process that may not be frequency resolved.

The low frequency region exhibited features similar to a Warburg element (Z_w) that describes semi-infinite diffusion. However

Table 3
Electrical conductivity of VB_2 materials and starting materials.

Sample		Electrical conductivity (S cm^{-1})
Vanadium powder		430 ± 77
Boron powder		$7 \pm 3 \times 10^{-4}$
Macroscopic VB_2	Uncoated	97 ± 5
	Coated	67 ± 14
Nanoscopic VB_2	Uncoated	230 ± 33
	Coated	90 ± 32

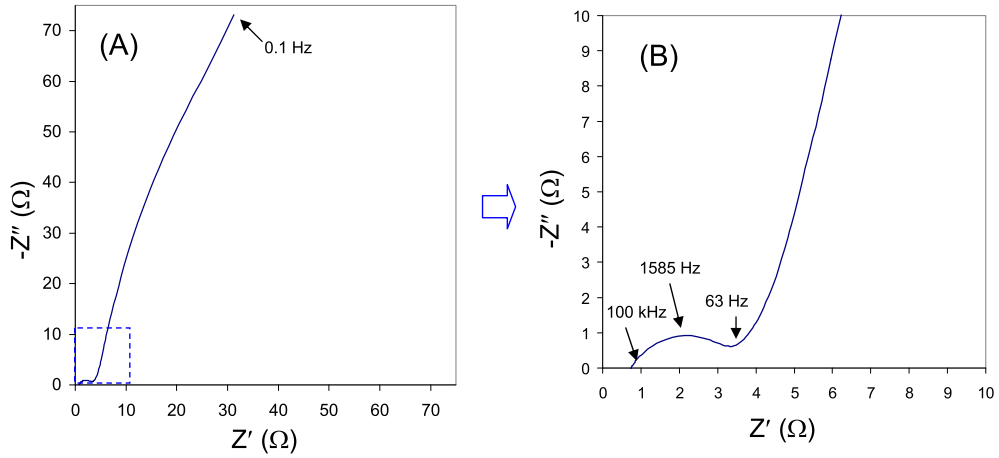

Fig. 5. Electrochemical impedance of nanoscopic, charged VB_2/air battery: (A) full frequency region; (B) expanded view of high frequency region.

in fitting the low frequency region, a Warburg element alone was not sufficient to obtain a reasonable fit of the experimental data. As observed with the Fig. 6, the low frequency region is not entirely a straight line, but also shows some curvature. The low frequency region was therefore fit with a combination of a resistor (R_2), a constant phase element (Q_2), and a Warburg element.

The resistance R_2 is attributed to resistances within the air cathode [17–19,22]. A constant phase element was also used for this region rather than a capacitor based on the distribution of capacitances within the air electrode. The Warburg element may be influenced by processes within the air cathode as well as the VB_2 anode. Previous work supports that diffusion of ions within the air electrode contributes to the Warburg element [17]. Within Zn–alkaline cells, the Warburg element has been also attributed to diffusion of soluble ionic species from the electrode surface to the bulk of solution [20]. The understanding of the processes associated with the various elements of the equivalent circuit (Fig. 6) was used to interpret the experimental data.

The electrochemical impedance data was obtained for the VB_2/air cells in charged and discharged states. Shown in Fig. 7 are the complex (Nyquist) impedance plots of (a) VB_2/air cells containing macroscopic VB_2 in the charged state and after discharge, and (b) VB_2/air cells containing nanoscopic VB_2 in the charged state and after discharge. From the experimental impedance data and the equivalent circuit described above, the values for R_s, R_1, Q_1, R_2, Q_2, and Z_w were obtained from fitting and are presented in Table 4.

The series resistances, R_s, for the charged cells containing either macroscopic or nanoscopic VB_2 are similar. This is consistent with our understanding that the electrolyte resistances within these two configurations are similar based on the same electrolyte composition (4 M NaOH/4 M KOH) and the cell configuration being utilized. The value of R_s for the charged cells is similar to the value obtained from the fitting of impedance data for Zn/air cells containing alkaline electrolytes [18]. The series resistance, R_s, increases from charge to discharge for both the macroscopic and the nanoscopic materials. The increase in R_s from charge to discharge is consistent with the formation of soluble discharge products in the electrolyte that increase the resistivity of the electrolyte [5,6]. The discharged

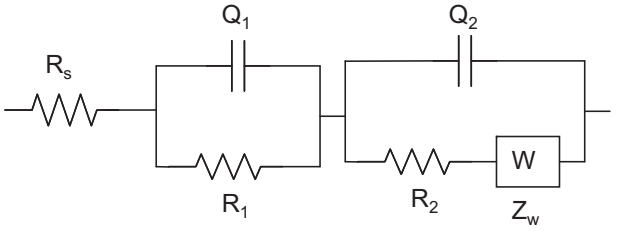

Fig. 6. Equivalent circuit used for fitting electrochemical impedance.

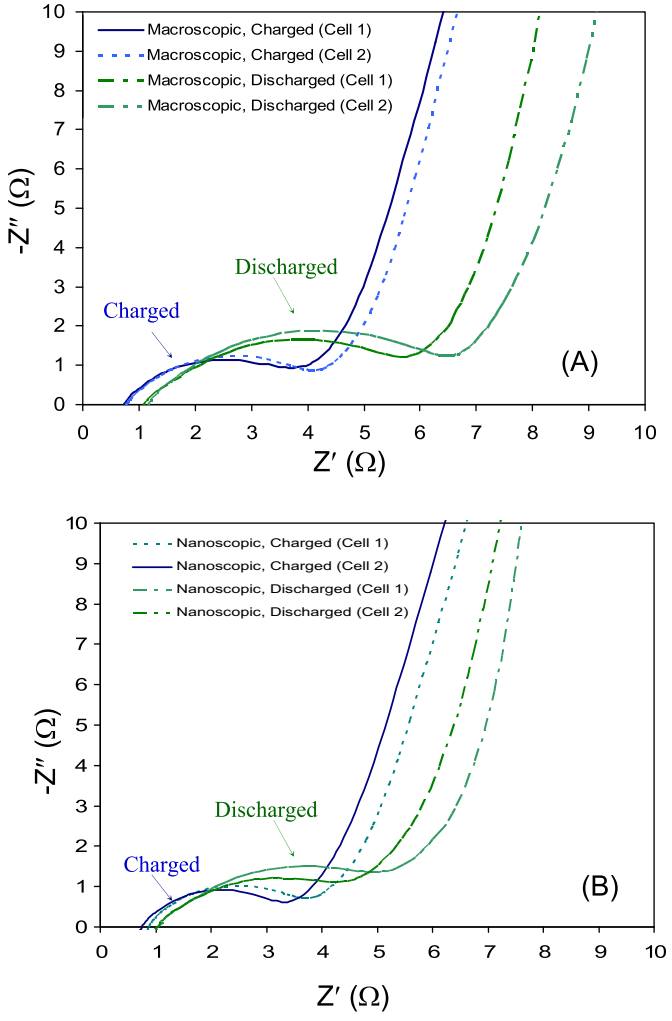

Fig. 7. Electrochemical impedance in the high frequency region of 5 mAh VB_2–air cells discharged at a constant load of 1000 Ω; (A) cells containing macroscopic 1.9% ZrO_2-coated VB_2 before and after discharge; (B) cells containing nanoscopic 1.9% ZrO_2-coated VB_2 before and after discharge.

Table 4
Parameters obtained from fitting of electrochemical impedance of VB_2–air cells using equivalent circuit as described in the text. *R* is resistance, *Q* denotes a constant phase element with the frequency power *n*, and Z_w is a Warburg element.

Sample		R_s (Ω)	R_1 (Ω)	Q_1 (S s^n) (n)	R_2 (Ω)	Q_2 (S s^n) (n)	Z_w (Ω^{-1} $s^{1/2}$)
Macroscopic VB_2	Charged	0.74	3.6	1.2×10^{-2} (0.9)	4770	6.3×10^{-4} (0.7)	7.1×10^{-7}
	Discharged	0.94	5.9	7.0×10^{-3} (0.9)	720	5.3×10^{-4} (0.7)	3.3×10^{-7}
Nanoscopic VB_2	Charged	0.68	3.5	1.7×10^{-2} (0.8)	1000	7.1×10^{-4} (0.7)	6.1×10^{-7}
	Discharged	0.99	5.9	3.7×10^{-3} (0.9)	3900	9.9×10^{-4} (0.6)	1.2×10^{-5}

nanoscopic VB_2 and macroscopic cells show similar values for the series resistance, R_s, upon discharge which suggests that similar discharge products and concentrations of discharge products may be present in the electrolyte.

Comparing the charge transfer resistances (R_1) for the nanoscopic and macroscopic materials, the nanoscopic material shows slightly lower resistances for the charged cells. The lower resistance may be attributed to the higher conductivity of the nanoscopic VB_2 material compared with the macroscopic VB_2 material. The clear trend from the impedance data is that the charge transfer resistance, R_1, increases from charge to discharge for cells containing both the macroscopic and the nanoscopic materials. The increase in the charge transfer resistance from charge to discharge indicates that the resistance associated with the charge transfer process changes as a function of the state of discharge, which may be due to material, surface, and/or electrolyte changes occurring during the discharge process. It is likely that the conductivity of the discharge product is substantially less than that of the VB_2 as will be probed in an upcoming study.

The additional resistor, R_2, is attributed primarily to resistances within the air cathode including resistance associated with ion transport to the catalyst sites. Within the experimental data, this resistance occurs in the low frequency region and captures the curvature present at low frequencies. The relatively high value of R_2 may be influenced by the electrolyte wetting, the ambient humidity, and the electrode architecture. Alkaline air cathodes, typically contain carbon and a catalyst such as manganese dioxide (MnO_2) and related compounds. Previous work involving impedance analysis of MnO_2 nanoarchictectures showed that the low frequency impedance response and the Warburg element were affected by the humidity [23]. The Warburg element can be correlated with the ion diffusion coefficient, however further analysis of the low frequency impedance region of the commercial air cathode was not performed based on the primary focus on the VB_2 anode material.

3.6. Towards practical VB_2/air batteries

In all batteries, the capacity of a practical cell is considerably less than the intrinsic, theoretical cell capacity. In our prior estimate of practical (compared to intrinsic) VB_2/air cell capacities, we extrapolated the similar case of zinc/air batteries that have achieved over 18% of the intrinsic capacity [6]. The practical capacity of air batteries is less than the intrinsic capacity for several reasons, such as inclusion of the cell casing, the air cathode current collector volume, and the volume expansion as the anode material combines with oxygen. This latter expansion is normally either designed within the anode compartment volume [3] or is part of the volume used to contain the electrolyte and can include the degree of hydration of the discharge products. For example, in discharging a Zn/air battery, the relative inverse density of the active anode material and its products are respectively: 0.14 cm^3 g^{-1} (Zn), 0.18 cm^3 g^{-1} (ZnO) and 0.33 cm^3 g^{-1} ($Zn(OH)_2$). The molar volume change of an air battery can be even greater, which for Zn/air changes from 9 cm^3 mol^{-1} (Zn) to 15 cm^3 mol^{-1} (ZnO) to 33 cm^3 mol^{-1} ($Zn(OH)_2$). For VB_2 and its oxidation products the relative densities are: 5.1 g cm^{-3} (VB_2), 3.36 g cm^{-3} (V_2O_5), and 2.55 (crystalline) or 1.84 (amorphous) g cm^{-3} (B_2O_3). Volume expansion of the VB_2/air cell is expected based on the addition of oxygen within the cell and the lower density of the discharge products, and the cell can be designed to accommodate the volume expansion in a manner similar to the construction of Zn/air batteries [3]. The discharge products are soluble species, [5,6] and the hydroxides of these V_2O_5 and B_2O_3 salts have been less characterized. We are currently exploring the degree of hydration and volume of the VB_2/air discharge products with the depth of discharge, and these will be the topic of a future publication.

4. Conclusions

The demands of emerging technologies have resulted in the need for a high capacity battery that can be rapidly discharged. The VB_2/air system provides extremely high energy density batteries. This work furthers our understanding of the performance of VB_2/air batteries at rapid discharge times and provides insight into the factors influencing the electrochemical properties and performance.

The data obtained in this work shows that for all discharge times evaluated, cells containing nanoscopic VB_2 anodes provide significantly higher voltages than cells containing macroscopic VB_2 anodes. For discharge times of ca. 4 h and longer, cells containing nanoscopic VB_2 show higher capacities than cells containing macroscopic VB_2. From the comparison of the nitrogen physisorption, electrical conductivity measurements and electrochemical performance, we determined that the higher performance of the VB_2 nanoscopic material compared with the macroscopic VB_2 material may result from the combination of the nanomaterial's higher surface area and higher electronic conductivity. The higher voltages may be attributed to the higher conductivity of the nanoscopic material, and the higher capacities may result from the higher surface area of the nanoscopic material, which allows a greater degree of material utilization. The coated nanoscopic VB_2 material has a surface area that is two orders of magnitude higher than the coated macroscopic VB_2 material. The higher voltage of the nanoscopic materials may also result from a more disordered structure, as supported by the broader X-ray diffraction peaks compared with macroscopic VB_2 [7]. At high discharge times of ca. $\leq$2 h, nanoscopic VB_2 and macroscopic VB_2 show similar capacities. This observation may point to a surface area limited discharge reaction process.

Transmission electron microscopy and energy dispersive X-ray spectroscopy were used to determine that the VB_2 nanomaterial is coated with a nanoscale zirconia layer, which may allow rapid discharge through the coating. Electrochemical impedance spectroscopy was used to analyze the cells before and after discharge and corroborated the lower resistance of the nano-VB_2 electrodes. The impedance results indicated that the charge transfer resistance changes during the discharge processes which suggests that the anode structure and properties change during the discharge.

These results provide a basis for further development of the unique multi-electron discharge process of VB_2, and the development of high energy and power density VB_2/air batteries. This work points to the development of higher surface area

materials to further improve the rate capabilities of VB_2/air batteries. Higher surface area materials may also be more susceptible to corrosion by the electrolyte, so developing an optimal protective and conductive coating will also be necessary. In addition to higher surface area materials, the design of electrode surfaces and electrolyte compositions may facilitate controlling the charge transfer resistances during the discharge process. Additional analysis of the discharge process and surface structure will facilitate the further development of high performance VB_2/air batteries for numerous applications.

Acknowledgements

The authors would like to gratefully acknowledge funding from the National Science Foundation (Award 1006568) and the Air Force Research Laboratory (Contract No. FA8650-11-M-5170) for support of this research.

Appendix A. Supplementary material

Supplementary material associated with this article can be found, in the online version, at http://dx.doi.org/10.1016/j.jpowsour.2013.03.071.

References

[1] Z. Rogulski, A. Czerwiński, J. Solid State Electrochem. 7 (2003) 118–121.
[2] V. Neburchilov, H. Wang, J.J. Martin, W. Qu, J. Power Sources 195 (2010) 1271–1291.
[3] D. Linden, T.B. Reddy, Handbook of Batteries, 3rd ed., McGraw-Hill, New York, 2002.
[4] X.-P. Gao, H.-X. Yang, Energy Environ. Sci. 3 (2010) 174–189.
[5] H.X. Yang, Y.D. Wang, X.P. Ai, C.S. Cha, Electrochem. Solid-State Lett. 7 (2004) A212–A215.
[6] S. Licht, H.M. Wu, X.W. Yu, Y.F. Wang, Chem. Commun. 3257–3259 (2008).
[7] S. Licht, C. Hettige, J. Lau, U. Cubeta, H. Wu, J. Stuart, B. Wang, Electrochem. Solid-State Lett. 15 (2012) A1–A3.
[8] S. Licht, S. Ghosh, B. Wang, D. Jiang, J. Asercion, H. Bergmann, Electrochem. Solid-State Lett. 14 (2011) A83–A85.
[9] S. Licht, X. Yu, D. Zheng, Chem. Commun. (2006) 4341.
[10] S. Licht, C. Hettige, J. Lau, U. Cubeta, H. Wu, J. Stuart, B. Wang, J. Electrochem. Soc. 155 (2008) 3257–3259.
[11] S. Licht, C. Hettige, J. Lau, U. Cubeta, H. Wu, J. Stuart, B. Wang, J. Electrochem. Soc. 155 (2008) A297–303.
[12] B.A. Holmberg, Y. Yan, J. Electrochem. Soc. 153 (2006) A146–A149.
[13] M.J. Bleda-Martinez, D. Lozano-Castello, D. Cazorla-Amoros, E. Morallon, Energy Fuels 24 (2010) 3378–3384.
[14] S. Licht, X. Yu, Y. Wang, J. Electrochem. Soc. 155 (1) (2008) A1–A7.
[15] E. Frackowiak, Phys. Chem. Chem. Phys. 9 (2007) 1774–1785.
[16] F. Pico, C. Pecharroman, A. Anson, M.T. Martinez, J.M. Rojo, J. Electrochem. Soc. 154 (2007) A579–A586.
[17] G.Q. Zhang, X.G. Zhang, H.L. Li, J. Solid State Electrochem. 10 (2006) 995–1001.
[18] S.M. Zhu, Z. Chen, B. Li, D. Higgins, H.J. Wang, H. Li, Z.W. Chen, Electrochim. Acta 56 (2011) 5080–5084.
[19] Z. Chen, A.P. Yu, R. Ahmed, H.J. Wang, H. Li, Z.W. Chen, Electrochim. Acta 69 (2012) 295–300.
[20] A. El-Sayed, H.S. Mohran, H.M. Abd El-Lateef, Metall. Mater. Trans. A 43 (2012) 619–632.
[21] M. Metikos-Hukovic, S. Omanovic, J. Electroanal. Chem. 455 (1998) 181–189.
[22] D. Thiele, A. Züttel, J. Power Sources 183 (2008) 590–594.
[23] M.S. Doescher, J.J. Pietron, B.M. Dening, J.W. Long, C.P. Rhodes, C.A. Edmondson, D.R. Rolison, Anal. Chem. 77 (2005) 7924–7932.